Transformation Optics Approach to Plasmon-Exciton Strong Coupling in Nanocavities

Rui-Qi Li,[1,2] D. Hernángomez-Pérez,[1] F. J. García-Vidal,[1,3,†] and A. I. Fernández-Domínguez[1,*]

[1]*Departamento de Física Teórica de la Materia Condensada and Condensed Matter Physics Center (IFIMAC),
Universidad Autónoma de Madrid, E-28049 Madrid, Spain*
[2]*Key Laboratory of Modern Acoustics, MOE, Institute of Acoustics, Department of Physics, Nanjing University,
Nanjing 210093, People's Republic of China*
[3]*Donostia International Physics Center (DIPC), E-20018 Donostia/San Sebastián, Spain*

We investigate the conditions yielding plasmon-exciton strong coupling at the single emitter level in the gap between two metal nanoparticles. Inspired by transformation optics ideas, a quasianalytical approach is developed that makes possible a thorough exploration of this hybrid system incorporating the full richness of its plasmonic spectrum. This allows us to reveal that by placing the emitter away from the cavity center, its coupling to multipolar dark modes of both even and odd parity increases remarkably. This way, reversible dynamics in the population of the quantum emitter takes place in feasible implementations of this archetypal nanocavity.

Plasmon-exciton-polaritons (PEPs) are hybrid light-matter states that emerge from the electromagnetic (EM) interaction between surface plasmons (SPs) and nearby quantum emitters (QEs) [1,2]. Crucially, PEPs only exist when these two subsystems are strongly coupled; i.e., they exchange EM energy coherently in a time scale much shorter than their characteristic lifetimes. Recently, much attention has focused on PEPs, since they combine the exceptional light concentration ability of SPs with the extreme optical nonlinearity of QEs. These two attributes makes them promising platforms for the next generation of quantum nanophotonic components [3].

A quantum electrodynamics description of plasmonic strong coupling of a single QE has been developed for a flat metal surface [4], and isolated [5,6] and distant nanoparticles [7–9], where SP hybridization is not fully exploited. From the experimental side, in recent years, PEPs have been reported in emitter ensembles [10–13], in which excitonic nonlinearities are negligible [14–16]. Only very recently, thanks to advances in the fabrication and characterization of large Purcell enhancement nanocavities [17–19], far-field signatures of plasmon-exciton strong coupling for single molecules have been reported experimentally [20].

In this Letter, we investigate the plasmonic coupling of a single emitter in a paradigmatic cavity, thoroughly explored in the context of optical antennas thanks to its ability to confine EM fields at very deep subwavelength scales: the nanometric gap between two spherical-shaped metal particles [13,19,20]. We develop a quasianalytical approach that fully exploits the covariance of Maxwell equations and is based on the method of inversion [21]. Inspired by recent advances in transformation optics (TO) [22,23], this approach fully accounts for the rich EM spectrum that originates from SP hybridization across the gap.

Our theory, which is the first application of the TO framework for the description of quantum optical phenomena, yields quasianalytical insight into the Wigner-Weisskopf problem [24] for these systems, and enables us to reveal the prescriptions that nanocavities must fulfil to support single QE PEPs.

Figure 1(a) sketches the system under study: a two level system (with transition frequency ω_E and z-oriented dipole moment μ_E) placed at position z_E within the gap δ between two spheres of permittivity $\epsilon(\omega) = \epsilon_\infty - [\omega_p^2/\omega(\omega + i\gamma)]$, embedded in a matrix of dielectric constant ϵ_D [see Supplemental Material (SM) [25] for further details]. We assume that the structure is much smaller than the emission wavelength and operate within the quasistatic approximation. The details of our treatment of SP-QE coupling in this geometry can be found in the SM. Briefly, by inverting the structure with respect to a judiciously chosen point [z_0 in Figure 1(a)], the spheres map into an annulus geometry in which the QE source and scattered EM fields are expanded in terms of the angular momentum l. This allows us to obtain the scattering Green's function, $G_{zz}^{sc}(\omega)$, in a quasianalytical fashion.

First we test our approach by analyzing the spontaneous emission enhancement experienced by an emitter at the gap center. Figure 1(b) plots the Purcell factor $P(\omega) = 1 + (6\pi c/\omega)\mathrm{Im}\{G_{zz}^{sc}(\omega)\}$ for dimers with $R_{1,2} = R$. To compare different sizes, $P(\omega)$ is normalized to R^{-3}. Black solid line plots the TO prediction (identical for all sizes), and color dots render full EM calculations (Comsol *Multiphysics*). At high frequencies, quasianalytics and simulations are in excellent agreement for all R. At low frequencies, discrepancies caused by radiation effects are evident for $R \gtrsim 30$ nm. The insets in Figure 1(b) render induced charge density maps for the four lowest peaks in
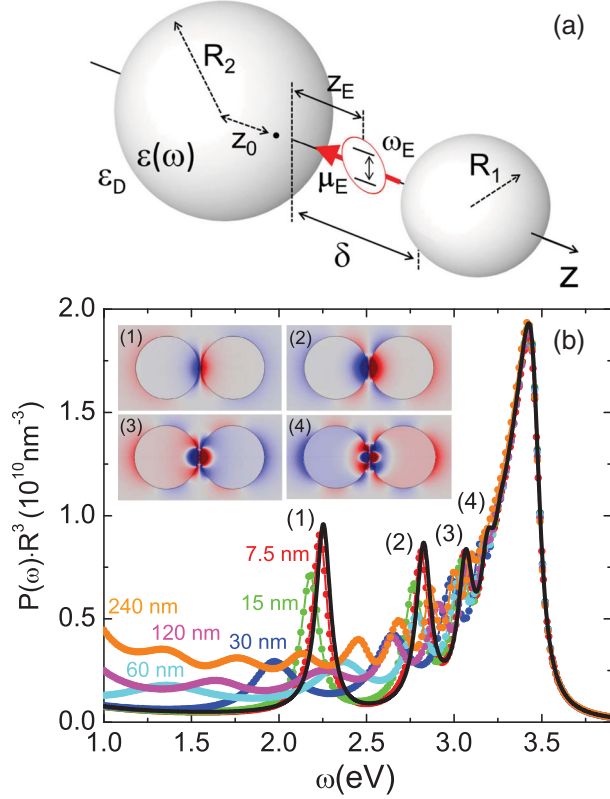
FIG. 1. (a) QE placed at the gap between two metal spheres of permittivity $\epsilon(\omega)$ and embedded in a dielectric medium ϵ_D. The QE dipole strength, position, and frequency are μ_E, z_E, and ω_E. (b) Normalized Purcell factor at the gap center for $R_{1,2} = R$ and $\delta = R/15$. Color dots: EM simulations for different R. Black line: TO prediction. Insets: induced charge distribution for the lowest 4 SP modes discernible in the spectrum (color scale is saturated for clarity).
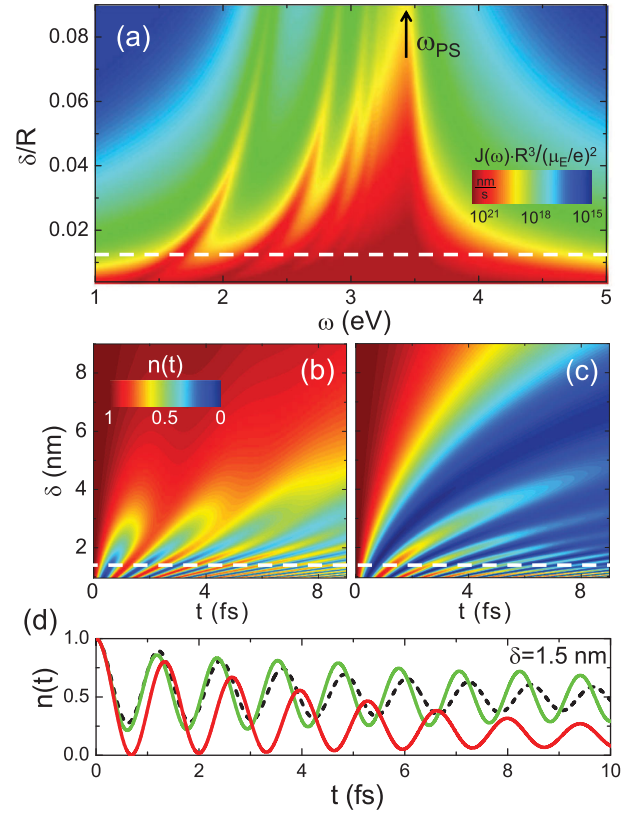
FIG. 2. (a) Normalized $J(\omega)$ at the gap center versus frequency and δ/R. (b),(c) $n(t)$ versus time and gap size for $R = 120$ nm and $\mu_E = 1.5\ e$ nm. The QE is at resonance with the dipolar SP mode in (b) and with the pseudomode in (c). (d) $n(t)$ for $\delta = 1.5$ nm (see white dashed lines) and two ω_E: 1.7 (green) and 3.4 (red) eV. Black dotted line corresponds to $\omega_E = 1.7$ eV obtained through the fitting of $J(\omega)$ at ω_{PS}.

the TO spectrum. These can be identified as SP resonances of increasing multipolar order. We can infer that the maximum that dominates all the spectra in Figure 1(b) is caused by the pseudomode (ω_{PS}) emerging from the spectral overlapping of higher order SPs [16]. Importantly, these are darker (weakly radiative) modes strongly confined at the gap region, which explains why our quasistatic description is valid at ω_{PS} even for $R = 240$ nm.

Now we investigate the spectral density across the gap cavity. This magnitude governs SP-QE interactions (see below), and can be expressed as $J(\omega) = (\mu_E^2 \omega^3 / 6\pi^2 \epsilon_0 \hbar c^3) P(\omega)$. Figure 2(a) shows TO-$J(\omega)$ evaluated at $z_E = \delta/2$ and normalized to μ_E^2/R^3 for different δ/R. For small gaps, the spectral density is maximized, and the contribution from different SPs is apparent. For larger gaps, $J(\omega)$ decreases, all maxima blue-shift and eventually merge at the pseudomode position. Importantly, Fig. 2(a) shows a universal trend, valid for all QEs and R (within the quasistatic approximation). Therefore, for a given δ/R, large μ_E and small R must be used to increase plasmon-exciton coupling.

Once the spectral density is known, the Wigner-Weisskopf problem [24] can be solved. It establishes that the equation governing the dynamics of the excited-state population, $n(t) = |c(t)|^2$, for an initially excited QE is

$$\frac{d}{dt} c(t) = -\int_0^t d\tau \int_0^\infty d\omega J(\omega) e^{i(\omega_E - \omega)(t-\tau)} c(\tau). \quad (1)$$

Figures 2(b) and 2(c) render the QE population at the center of the cavity in panel (a) as a function of time and gap size. The spheres radius is 120 nm (so that $1 \lesssim \delta \lesssim 10$ nm), and $\mu_E = 1.5\ e$ nm (InGaN/GaN quantum dots at 3 eV [30]). The emitter is at resonance with the lowest (dipolar) SP (b) and with the pseudomode (c) maxima in Fig. 2(a), respectively. Note that the former disperses with gap size, whereas $\omega_E = \omega_{PS}$ for the latter. We can observe that both configurations show clear oscillations in $n(t)$, which indicates that coherent energy exchange is taking place. In this regime, strong coupling occurs, and the nanocavity supports PEPs. However, for $\delta > 3$ nm, the reversible dynamics in the population is lost in both panels; QEs

and SPs are only weakly coupled, and $n(t)$ follows a monotonic decay.

Figure 2(d) plots $n(t)$ at strong coupling, $\delta = R/80 = 1.5$ nm [see white dashed lines in panels (a)–(c)]. The red (green) line corresponds to QE at resonance with the pseudomode (dipolar SP) peak. The excited state population obtained from the fitting of $J(\omega)$ around ω_{PS} and evaluated at the lowest SP frequency is shown as a black dashed line. The similarity between solid green and dashed black lines implies that the population dynamics is fully governed by the pseudomode, even when the two maxima in $J(\omega)$ are far apart [the differences between Figs. 2(b) and 2(c) originate from detuning effects]. This fact enables us to extend the validity of our approach to larger structures, as radiative effects do not play a significant role at the pseudomode. More importantly, our findings reveal that QE strong coupling in nanocavities does not benefit from highly radiative plasmonic modes despite their low resonant frequencies and associated low sensitivity to metal absorption.

We have found that $R = 120$ nm cavities can support single QE PEPs only if $\delta < 4$ nm. Similar calculations for single particles (not shown here) indicate that the onset of strong coupling takes place at similar distances, $z_E \lesssim 2$ nm. This means that the configuration investigated so far does not exploit cooperative effects between the nanospheres, associated with the enhancement in $J(\omega)$ expected from SP hybridization. To verify this, Fig. 3(a) plots $J(\omega_{PS})$ versus δ evaluated at the center of the cavity and normalized to twice the maximum in the spectral density for an isolated sphere ($R = 120$ nm, $z_E = \delta/2$). Whereas normalized $J(\omega_{PS})$ is much larger than 1 for $\delta = 1.5$ nm, it decays to ~0.5 for gaps larger than 4 nm. Therefore, only very small gap cavities take advantage of SP hybridization. The inset of Fig. 3(a) plots $J(\omega)$ for 120 nm radius dimer (blue) and single sphere (green) evaluated at $z_E = 4$ nm, showing that the maximum spectral density is very similar in both cases.

We explore next the effect that moving the QE away from the gap center has on the cavity performance. We consider $\delta = 8$ nm, for which strong coupling does not take place at $z_E = \delta/2$; see Figs. 2(b) and 2(c). Figure 3(b) plots $J(\omega_{PS})$ versus z_E for two different normalizations. Black dashed line shows the ratio of $J(\omega_{PS})$ and its value at $z_E = \delta/2$. We can observe that the spectral density maximum grows exponentially as the QE approaches one of the particles, yielding factors up to 10^3. This effect could be attributed to the stronger interaction with the SPs supported by the closest sphere. To test this, red solid line plots $J(\omega_{PS})$ now normalized to the sum of the spectral densities calculated for each of the spheres isolated and evaluated at z_E and $\delta - z_E$. Remarkably, enhancements up to 10^2 are found in this asymmetric configuration. Therefore, the pronounced increase of $J(\omega)$ cannot be simply caused by proximity effects, but it must be due to a significant enhancement of the cooperativity between the two nanoparticles. Figure 3(c) plots $n(t)$ for three z_E values
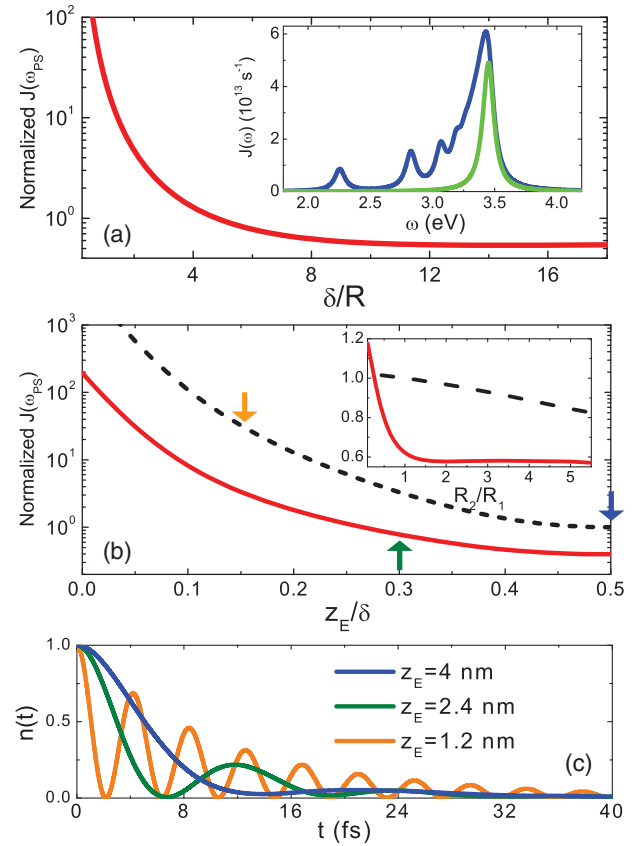

FIG. 3. (a) $J(\omega)$ at $z_E = \delta/2$ and $\omega_E = \omega_{PS}$ versus δ normalized to the sum of the spectral density maxima for the spheres isolated. Inset: $J(\omega)$ for the dimer (blue) and isolated particle (green) for $\delta = 8$ nm, $R = 120$ nm. (b) Spectral density at the pseudomode versus z_E/δ. Red solid line: $J(\omega_{PS})$ normalized to the sum of the two spheres isolated. Black dashed line: $J(\omega_{PS})$ normalized to its value at $z_E = \delta/2$. Inset: Same but versus the ratio R_2/R_1 for $z_E = \delta/2$. (c) $n(t)$ for $\omega_E = \omega_{PS}$ and three z_E values ($\mu_E = 1.5$ e nm).

[indicated by vertical arrows in panel (b)], proving that strong coupling occurs for z_E far from the cavity center. The inset of Fig. 3(b) investigates if SP-QE coupling can benefit further from geometric asymmetry. It renders $J(\omega_{PS})$ versus R_2/R_1 for both normalizations, and proves that the cavity performance is rather independent of the particle sizes in the regime $R_{1,2} \gg \delta$.

To gain physical insight into the dependence of $J(\omega)$ on the QE position, we assume that $\delta \ll R_{1,2}$, and work within the high quality resonator limit [6]. This way, we can obtain analytical expressions for $J(\omega)$, which can be written as a sum of Lorentzian SP contributions of the form

$$J(\omega) = \sum_{l=0}^{\infty} \sum_{\sigma=\pm 1} \frac{g_{l,\sigma}^2}{\pi} \frac{\gamma/2}{(\omega - \omega_{l,\sigma})^2 + (\gamma/2)^2}, \quad (2)$$

where the index l can be linked to the multipolar order of the SP, σ to its even ($+1$) or odd (-1) character, and γ is the damping parameter in $\epsilon(\omega)$.
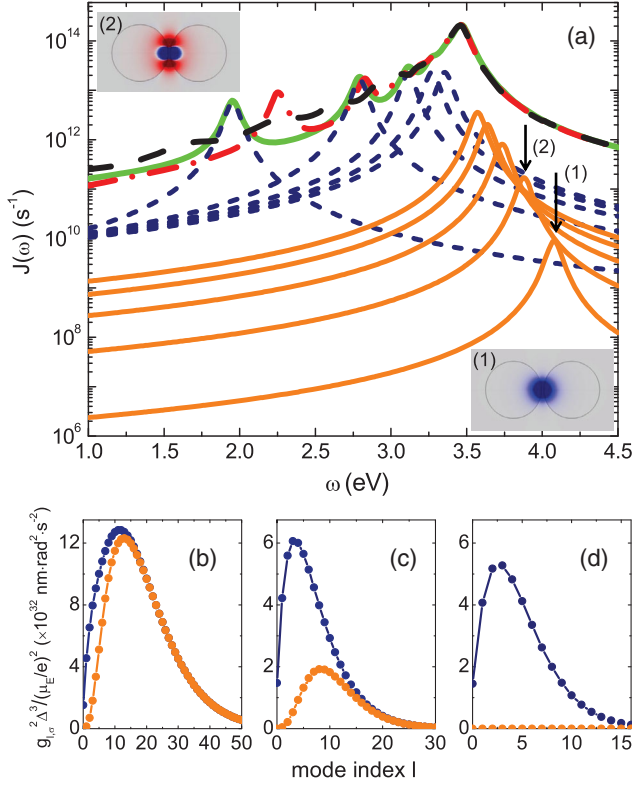
FIG. 4. (a) Spectral density for $z_E = 2.4$ nm obtained through numerical (black dashed line), exact TO (red dotted-dashed line), and analytical TO (solid green line) calculations. The contribution to $J(\omega)$ due to even and odd modes are plotted in dark blue dotted and solid orange lines, respectively. Inset: surface charge map for the two lowest odd SPs. (b) Normalized coupling constant squared for even and odd modes versus l for z_E: 1.2 nm (b), 2.4 nm (c), and 4 nm (d).

The SP resonant frequencies in Eq. (2) have the form

$$\omega_{l,\sigma} = \frac{\omega_p}{\sqrt{\epsilon_\infty + \epsilon_D \frac{\xi_l + \sigma}{\xi_l - \sigma}}}, \qquad (3)$$

with $\xi_l = [(3R + \delta - z_0)(R + \delta - z_0)/(R - z_0)(R + z_0)]^{l+\frac{1}{2}}$. Note that, for simplicity, we focus here in the case $R_{1,2} = R$, but general expressions can be found in the SM. Importantly, for large l, $\xi_l \gg 1$, which enables us to write $\omega_{PS} \sim (\omega_p/\sqrt{\epsilon_\infty + \epsilon_D})$. The spectral overlapping giving rise to the pseudomode always peaks at a frequency slightly lower than the SP asymptotic frequency for a flat metal surface.

The coupling constants, $g_{l,\sigma}$, in Eq. (2) are mathematically involved functions of the geometric parameters of the cavity. However, without loss of generality, we can write

$$g_{l,\sigma}^2 = \frac{\mu_E^2}{\Delta^3} f\left(\frac{\Delta}{z_E + R - z_0}\right), \qquad (4)$$

where $f(\cdot)$ contains all the dependence on the emitter position and $\Delta = (R + \delta - z_0)(3R + \delta - z_0)/(2R + \delta - z_0)$

gives the inverse volume scaling of $J(\omega)$ anticipated in Fig. 1. Equation (4) proves formally that the cavity performance can be improved by reducing its overall size, as this increases the coupling strength for all SP modes. Let us remark that the analytical decomposition of $J(\omega)$ given by Eqs. (2)–(4) proves the suitability of TO for the description of quantum nano-optical phenomena. It provides naturally a convenient and efficient quantization of EM fields in lossy, complex nanocavities, a research area of much theoretical activity lately [31,32].

In the following, we test our analytical approach. Figure 4(a) plots $J(\omega)$ for the case $z_E = 0.3\delta$ in Fig. 3(c). Red dashed-dotted and black dashed lines plot exact TO and EM calculations, respectively. The spectrum obtained from Eq. (2) is rendered as the green solid line. It reproduces $J(\omega)$ satisfactorily except for a small red-shift in the lowest frequency peak (with respect to the exact TO prediction). The various contributions to $J(\omega)$ in Eq. (2) are plotted in blue dashed and solid orange lines in Fig. 3(a). These two sets correspond to even ($\sigma = +1$) and odd ($\sigma = -1$) SP modes, respectively. Note that the former (latter) blue-shifts (red-shifts) towards ω_{PS} for increasing l. These different trends originate from the ratio $(\xi_l + \sigma)/(\xi_l - \sigma)$ in the denominator of Eq. (4), which is always larger (smaller) than 1 for $\sigma = +1$ ($\sigma = -1$). The insets of Fig. 4(a) depict induced surface charge density maps for the maxima corresponding to the two lowest odd SP contributions. Note that due to their antisymmetric character, these are purely dark, dipole-inactive, modes in the quasistatic limit.

Figures 4(b)–(d) plot Eq. (4) for both SP symmetries as a function of the mode index l and evaluated at the three z_E's in Fig. 3(c). For QEs in close proximity to one of the particles ($z_E = 0.15\delta$), $g_{l,\pm 1}^2$ are largest. The coupling strength dependence on l is very similar for both mode symmetries and peaks at $l \simeq 12$. This indicates that high multipolar dark SPs are responsible for the main contributions to $J(\omega)$. At intermediate positions, $z_E = 0.3\delta$, both coupling constants decrease, being the reduction much more pronounced in $g_{l,-1}^2$. Finally, $g_{l,-1}^2$ vanishes at the cavity center ($z_E = 0.5\delta$), and the QE interacts only with even SPs having $l \sim 3$. The bright character of these plasmon resonances translates into an increase of radiative losses, which worsens significantly the cavity performance. Figures 4(b)–(d) evidence that the remarkable (several orders of magnitude) enhancement in $J(\omega_{PS})$ shown in Fig. 3(b) for z_E away from the $\delta/2$ is caused by two different mechanisms. On the one hand, the emitter interacts more strongly with even SPs (of increasing multipolar order). On the other hand, it can couple to a whole new set of dark modes contributing to $J(\omega)$, those with odd symmetry, which are completely inaccessible for $z_E = \delta/2$. It is the combination of these two effects which makes possible for one to realize plasmon-exciton strong coupling in nanocavities with $\delta \sim 5 - 10$ nm.

Finally, in order to prove the predictive value of our analytical method, we calculate the plasmon-exciton coupling strength for geometrical and material parameters modeling the experimental samples in Ref. [20] (see SM for details). Our approach predicts $g_{0,+1} = 19$ meV for the dipolar SP mode, and $g_{\mathrm{PS}}^{\mathrm{eff}} = 120$ meV for the pseudomode. The latter is in good agreement with the measured value: $g_{\exp} = 90$ meV. This indicates that, in accordance with our theoretical findings, high order multipolar dark modes seem to play a relevant role in the QE-SP interactions taking place in the nanocavity samples that lead to single molecule strong coupling.

In conclusion, we have presented a transformation optics description of plasmon-exciton interactions in nanometric gap cavities. We have shown that it is the dark pseudomode that builds up from the spectral overlapping of high frequency plasmonic modes which governs the energy exchange between emitter and cavity field. The quasianalytical character of our approach allows for a thorough exploration of these hybrid systems, revealing that the coupling can be greatly enhanced when the emitter is displaced across the gap. We have obtained analytical expressions that prove that this increase of the spectral density in asymmetric positions is caused by not only even, but also odd modes. Finally, we have verified the predictive value of our analytical approach against recent experimental data, which demonstrates its validity as a design tool for nanocavities sustaining plasmon-exciton-polaritons at the single emitter level.

[*] a.fernandez-dominguez@uam.es

[†] fj.garcia@uam.es

[1] D. E. Chang, A. S. Sorensen, P. R. Hemmer, and M. D. Lukin, Phys. Rev. Lett. **97**, 053002 (2006).

[2] P. Törmä and W. L. Barnes, Rep. Prog. Phys. **78**, 013901 (2015).

[3] M. S. Tame, K. R. McEnery, S. K. Özdemir, J. Lee, S. A. Maier, and M. S. Kim, Nat. Phys. **9**, 329 (2013).

[4] A. González-Tudela, P. A. Huidobro, L. Martín-Moreno, C. Tejedor, and F. J. García-Vidal, Phys. Rev. B **89**, 041402(R) (2014).

[5] A. Trügler and U. Hohenester, Phys. Rev. B **77**, 115403 (2008).

[6] E. Waks and D. Sridharan, Phys. Rev. A **82**, 043845 (2010).

[7] S. Savasta, R. Saija, A. Ridolfo, O. Di Stefano, P. Denti, and F. Borghese, ACS Nano **4**, 6369 (2010).

[8] A. Manjavacas, F. J. García de Abajo, and P. Nordlander, Nano Lett. **11**, 2318 (2011).

[9] R. Esteban, J. Aizpurua, and G. W. Bryant, New J. Phys. **16**, 013052 (2014).

[10] J. Bellessa, C. Bonnand, J. C. Plenet, and J. Mugnier, Phys. Rev. Lett. **93**, 036404 (2004).

[11] T. Schwartz, J. A. Hutchison, C. Genet, and T. W. Ebbesen, Phys. Rev. Lett. **106**, 196405 (2011).

[12] F. Todisco, S. D'Agostino, M. Esposito, A. I. Fernández-Domínguez, M. De Giorgi, D. Ballarini, L. Dominici, I. Tarantini, M. Cuscuna, F. D. Sala, G. Gigli, and D. Sanvitto, ACS Nano **9**, 9691 (2015).

[13] G. Zengin, M. Wersäll, S. Nilsson, T. J. Antosiewicz, M. Käll, and T. Shegai, Phys. Rev. Lett. **114**, 157401 (2015).

[14] A. Salomon, R. J. Gordon, Y. Prior, T. Seideman, and M. Sukharev, Phys. Rev. Lett. **109**, 073002 (2012).

[15] A. González-Tudela, P. A. Huidobro, L. Martín-Moreno, C. Tejedor, and F. J. García-Vidal, Phys. Rev. Lett. **110**, 126801 (2013).

[16] A. Delga, J. Feist, J. Bravo-Abad, and F. J. García-Vidal, Phys. Rev. Lett. **112**, 253601 (2014).

[17] S.-H. Gong, J.-H. Kim, Y.-H. Ko, C. Rodriguez, J. Shin, Y.-H. Lee, L. S. Dang, X. Zhang, and Y.-H. Cho, Proc. Natl. Acad. Sci. U.S.A. **112**, 5280 (2015).

[18] T. Hartsfield, W.-S. Chang, S.-C. Yanga, T. Ma, J. Shi, L. Sun, G. Shvets, S. Link, and X. Li, Proc. Natl. Acad. Sci. U.S.A. **112**, 12288 (2015).

[19] T. B. Hoang, G. M. Akselrod, and M. H. Mikkelsen, Nano Lett. **16**, 270 (2016).

[20] R. Chikkaraddy, B. de Nijs, F. Benz, S. J. Barrow, O. A. Scherman, E. Rosta, A. Demetriadou, P. Fox, O. Hess, and J. J. Baumberg, Nature (London) **535**, 127 (2016).

[21] L. D. Landau and E. M. Lifshitz, *Electrodynamics of Continuous Media* (Pergamon Press, Moscow, 1960).

[22] J. B. Pendry, A. Aubry, D. Smith, and S. A. Maier, Science **337**, 549 (2012).

[23] J. B. Pendry, A. I. Fernández-Domínguez, Y. Luo, and R. Zhao, Nat. Phys. **9**, 518 (2013).

[24] H.-P. Breuer and F. Petruccione, *The Theory of Open Quantum Systems* (Oxford University Press, Oxford, England, 2002).

[25] See Supplemental Material at http://link.aps.org/supplemental/10.1103/PhysRevLett.117.107401, which includes Refs. [26–29], for a comprehensive description of the TO theory and details of the calculations for experimental geometries.

[26] J. B. Pendry, Y. Luo, and R. Zhao, Science **348**, 521 (2015).

[27] R. Zhao, Y. Luo, A. I. Fernández-Domínguez, and J. B. Pendry, Phys. Rev. Lett. **111**, 033602 (2013).

[28] L. Novotny and B. Hecht, *Principles of Nano-Optics* (Cambridge University Press, Cambridge, England, 2012).

[29] A. Vial, A.-S. Grimault, D. Macías, D. Barchiesi, and M. Lamy de la Chapelle, Phys. Rev. B **71**, 085416 (2005).

[30] I. A. Ostapenko, G. Hönig, C. Kindel, S. Rodt, A. Strittmatter, A. Hoffmann, and D. Bimberg, Appl. Phys. Lett. **97**, 063103 (2010).

[31] M. B. Doost, W. Langbein, and E. A. Muljarov, Phys. Rev. A **90**, 013834 (2014).

[32] P. T. Kristensen and S. Hughes, ACS Photonics **1**, 2 (2014).